Fundamental interaction process between pure edge dislocation and energetically stable grain boundary

T. Tsuru,[1] Y. Shibutani,[2] and Y. Kaji[1]
[1]*Nuclear Science and Engineering Directorate, Japan Atomic Energy Agency, 2-4 Shirakata-Shirane, Tokai-mura, 319-1195 Ibaraki, Japan*
[2]*Department of Mechanical Engineering, Osaka University, 2-1 Yamadaoka, Suita, 565-0871 Osaka, Japan*
(Received 10 September 2008; published 14 January 2009)

The interaction between dislocations and grain boundaries is the principal factor for determining the mechanical properties and the plastic deformation behavior of metals. It is possible to control the grain-boundary microstructure and the macroscopic behavior has been widely exploited for scientific and industrial applications. In atomic scale, however, specific interaction characteristics such as the reaction energy and pathway have yet to be revealed. We have investigated the interaction process between a dislocation and an energetically stable grain boundary, and the quantitative characteristics were determined via atomistic transition state analysis. As a result, the interaction energy is found to be 1.16×10^{-1} eV/Å, which is 10^4 times higher than the Peierls potential. The lattice dislocations subsequently experience anomalous dissociations on the grain boundary, which becomes a key factor for the previously unexplained dislocation disappearance and grain-boundary migration.

DOI: 10.1103/PhysRevB.79.012104 PACS number(s): 61.72.Yx, 02.70.Ns, 61.72.Lk, 61.72.Mm

The dislocation–grain-boundary process is fundamental to the improvement of the mechanical properties of metallic materials. This process contributes significantly to plastic deformation as well as dislocation-dislocation interactions. These lattice defects have been effectively utilized for material strengthening as determined by the Hall-Petch relationship.[1,2] The detailed atomic structure of a low-angle grain boundary has been observed using high-resolution transmission electron microscopy (TEM).[3] Piled-up dislocations at grain boundaries, as well as the disappearance of dislocations from the interaction between the dislocations and the grain boundaries under indentation-induced stress, have been observed recently by *in situ* nanoindentation with TEM.[4,5] Computer simulations based on atomistic models have advanced over the last few decades and have allowed us to calculate the properties of typical coincidence site lattice (CSL). Basic properties of CSL grain boundaries, restricted to low-value CSLs such as $\Sigma3$ and $\Sigma5$, can be calculated by density-functional theory (DFT).[6] The effect of impurities in these low-sigma CSLs has been investigated.[7–9] Presently, DFT calculations have difficulty in correctly describing the dislocation–grain-boundary system. Atomistic simulations using empirical potentials have been used in a large number of studies of grain boundaries and dislocations. The equilibrium structures and corresponding grain-boundary energies of various kinds of tilt CSLs were investigated.[10] Monte Carlo simulations were carried out for the grain-boundary sliding process and vacancy effect.[11,12] Molecular-dynamics (MD) simulations have been performed to investigate the nanoscale plastic deformation.[13–15]

While polycrystalline materials used in actual equipment include various types of grain boundaries, the knowledge and information obtained by observations of the total system cannot be applied directly to nanoscale materials produced by recent miniaturization technology. The fundamental mechanisms of the interaction process between defect structures and individual crystal grain should thus be comprehensively examined. In focusing on the specific type of the CSL, the dislocation dissociation has been investigated by MD simulation.[16–19] They provide the detailed understanding of the dissociation of the Burgers vector of glide dislocation in the interaction process. On the other hand, these MD simulations have difficulty estimating a quantitative reaction property because they are performed under the several specific load conditions such as nanoindentation. In this study, we focused on the most stable symmetric CSL tilt $\Sigma3(\bar{1}11)[110]$ grain boundary in fcc aluminum. Grain-boundary energy is first evaluated comparing with other specific CSL grain boundaries. Then the interaction process in the simple system including a pure edge dislocation and a $\Sigma3(\bar{1}11)[110]$ grain boundary was quantitatively evaluated by atomistic transition state analysis, using the nudged elastic band (NEB) method.[20] The reaction energy and the transient interaction mechanism are thus discussed in relation to each other.

We first performed a sequence of structure stabilization calculations to obtain the grain-boundary energies of the $\langle110\rangle$ tilt CSL grain boundaries in fcc aluminum. Four CSL structures of $\Sigma3(\bar{1}11)[110]$, $\Sigma3(\bar{1}12)[110]$, $\Sigma11(\bar{3}32)[110]$, and $\Sigma11(\bar{1}13)[110]$ were constructed by a supercell model with a triaxial periodic boundary condition. Stable configurations are obtained by combining finite-temperature molecular dynamics and conjugate gradient (CG) energy minimization. The embedded atom method (EAM) type interatomic potential proposed by Mishin *et al.*[21] is employed. Stable structures were calculated for more than 70 atom layers at the normal to the grain-boundary plane. In this model the stress distribution, derived from the grain boundary, is localized within several atomic layers and therefore the interaction between boundaries within the supercell is negligibly small. The validity of the fundamental characteristics such as elastic constants using the EAM potential has been assessed in our previous study.[22] To verify the validity

TABLE I. Grain-boundary energy evaluated via EAM and DFT.

	Grain-boundary energy (mJ/m^2)			
	$\Sigma3(\bar{1}11)$	$\Sigma3(\bar{1}12)$	$\Sigma11(\bar{3}32)$	$\Sigma11(\bar{1}13)$
EAM	75.1	354.2	496.1	150.5
DFT-GGA	50.8	331.6	444.6	166.0

of the grain-boundary property, we performed *ab initio* DFT calculations using the Vienna *Ab initio* Simulation Package (VASP) (Refs. 23 and 24) with the Perdew-Wang generalized gradient approximation (GGA) exchange-correlation density functional[25] and the ultrasoft pseudopotential.[23] The total numbers of atoms used were 72, 86, 116, and 96. The cutoff energy for the plane-wave basis set is 300 eV. The following Brillouin-zone *k*-point samplings are chosen using the Monkhorst-Pack algorithm:[26] $9\times16\times1$, $7\times16\times1$, $4\times16\times1$, and $5\times16\times1$, respectively. The fully relaxed configurations are obtained by the CG method under a convergence condition of 0.02 eV/Å. The grain-boundary energies of CSL grain boundaries calculated by both EAM and DFT are shown in Table I. It is shown that the grain-boundary energies obtained by EAM potential correspond, both quantitatively and qualitatively, to the DFT calculations. $\Sigma3(\bar{1}11)[110]$ and $\Sigma11(\bar{1}13)[110]$ show extremely low grain-boundary energies and these are known as energy cusp grain boundaries. From a macroscopic point of view, the stability of the grain-boundary energy appears to contribute to the probability of dislocation absorption into grain boundary. However, in reality the dislocations interact with a stable CSL grain boundary to represent complicate local rearrangement of dislocations.

To evaluate the interaction between a dislocation and a grain boundary, the NEB method,[20] which is one of the atomistic transition state theories searching for the minimum-energy path (MEP), was used. We developed the parallel computing technique based on a message passing interface (MPI) via MASTER-SLAVE algorithm, which enabled us to treat large-scale atomic models for NEB simulations. For NEB, the initial and final states should be constructed. The initial-state model includes a pure edge dislocation separate from the grain boundary and it was constructed as follows. The two grains that have the most stable $\Sigma3$ grain boundary are first created according to the rotation angle. Rigid body rotation is applied to the grain-boundary model to direct the model in the directions of $x[\bar{1}10]$, $y[\bar{1}\bar{1}2]$, and $z[111]$. A pure edge dislocation with a Burgers vector of $(a/2)[\bar{1}10]$, where a is the lattice constant, is introduced on one side of the two grains. The atomistic model is shown in Fig. 1 and considered for a rectangular parallelepiped, containing approximately 550 000 atoms, which has dimensions of $40\times15\times15$ nm^3 aligned along the above-mentioned directions. The final states are generated by applying in-plane shear to the initial model and subsequently removing the shear. Both the initial and final states should be at their respective local minima for the deformation process during interaction between the dislocation and grain boundary. To evaluate the MEP, four equivalent layers as shown in Fig. 1 are considered. Each layer is extracted according to the unit length corresponding to atomic periodicity along the line-sense vector of the pure edge dislocation and is equal to $(\sqrt{6}/2)a$.

The reaction energy along the MEP for the dislocation–grain-boundary process is shown in Fig. 2(a), where reaction energy for a unit length of pure edge dislocation in each equivalent layer shown in Fig. 1 is collectively given. All curves show a negligibly small energy increment in the early stage of the reaction and they subsequently experience an abrupt increase midway through the reaction. The maximum value is equivalent to the activation energy for the interaction between a dislocation and the $\Sigma3$ grain boundary. The four activation energies are approximately equal while the reaction coordinates at the maximum values differ from one another, because the line-sense vector of the dislocation is not parallel to the grain-boundary plane and the interaction occurs in order of the layers I, II, III, and IV of Fig. 1. The activation energy ΔE is thus obtained as the average of the maximum values of four layers along the MEP and found to be 1.16×10^{-1} eV/Å. Preliminary NEB simulations have been done to obtain the Peierls potential for the pure edge dislocation in aluminum and we found that the Peierls potential is $E_{PN}=1.2\times10^{-5}$ eV/Å. We confirmed that the energy barrier for the interaction process is much higher than the Peierls potential (10^4 times) and thus the $\Sigma3(\bar{1}11)[110]$ CSL grain boundary is a major energy barrier for a mobile dislocation in the crystal grain. Total energies decrease as the reactions progress beyond the maxima, and the energy state of the final configuration is much lower than that of the initial configuration. A direct link, which is dependent on the reaction coordinate, is given by the atomic configuration of each replica image. Atomic configurations, which correspond to the referenced reaction coordinates (i)–(v) as indicated in Fig. 2(a), are shown in Fig. 2(b) where the images are produced by ATOMEYE.[27] Each atom is color coded according to the shear stress τ_{zx} normalized in the range $-1.5\leq\tau_{zx}\leq1.5$ GPa. In Fig. 2(b)(i), the pure edge dislocation is separate from the grain boundary. The dislocation then interacts with the grain boundary and the reaction energy reaches a maximum value at the moment of interaction [Fig. 2(b)(ii)]. After the dislocation interacts with the grain boundary a misfit is observed at the reaction site (dashed-dotted circle). Another misfit stress generated by the lattice defect is observed on the grain boundary and this defect structure moves along the grain-boundary plane [Figs. 2(b)(iii)–2(b)(v), dashed circle]. There are three interaction possibilities in the dislocation–grain-boundary process: absorption, reflection, and passage through the grain boundary.[28] These differences of the interaction modes depend on the types of grain boundaries such as CSL, low-angle, and random grain boundaries. These grain boundaries contribute significantly to the stress field in the vicinity of a boundary plane. In the case of a $\Sigma3$ grain boundary, the interaction process results from a local rearrangement due to a dislocation dissociation. The reaction energy may be described as the energy barrier required to trigger the dislocation dissociation beyond the repulsive stress. To understand the crystallographic aspect of the misfit dislocation dissociation, the misfit energy distributions at the

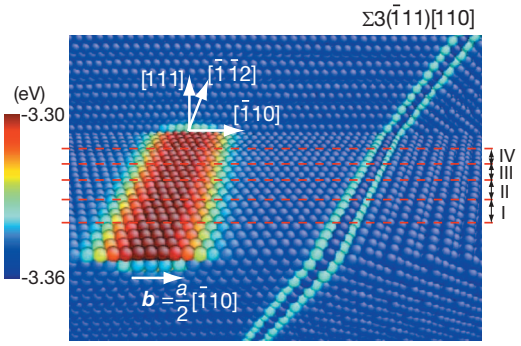

FIG. 1. (Color) The initial-state atomic configuration for the NEB simulation. The atomic model includes a pure edge dislocation and Σ3 CSL grain boundary, and the part of the system is cut out in a staircase pattern to emphasize two defect structures. Four equivalent layers with widths of $(\sqrt{6}/2)a$ are extracted to evaluate the reaction energies along MEP.

representative points in the interaction process corresponding to Fig. 2(a) [(i), (iii), and (v)] are shown in Fig. 3(a), which are created from the perspectives of both the direction of line-sense vector and the direction perpendicular to the grain boundary.

The grain-boundary plane migrates, as the misfit dislocation moves, by a unit width of the (111) plane which is equal

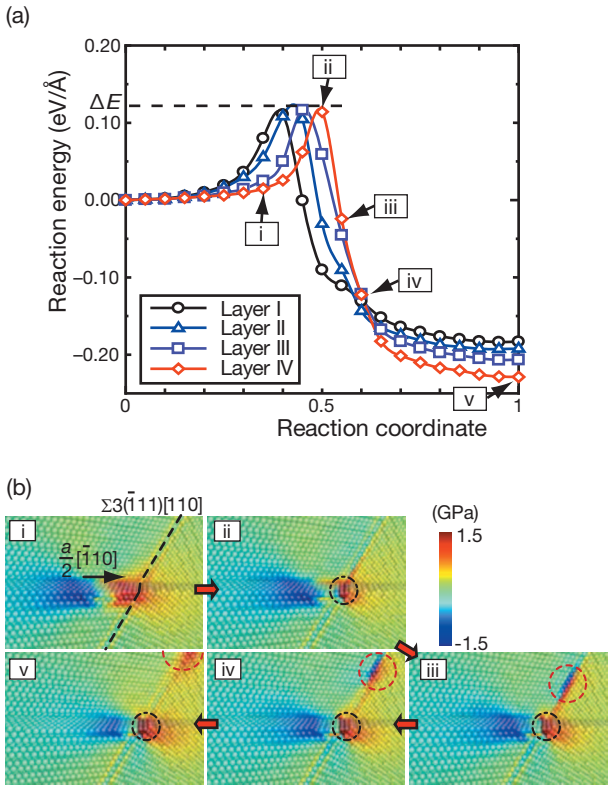

FIG. 2. (Color) Interaction process of an edge dislocation and a Σ3 grain boundary. (a) The reaction energies of four layers along the MEP of the interaction process per unit length of a dislocation. (b) Atomic configurations visualized by atomic shear stress τ_{zx} associated with the reference number represented in the reaction energy curve. Dissociated mobile and immobile dislocations are marked by dashed circle and dashed-dotted circle, respectively.

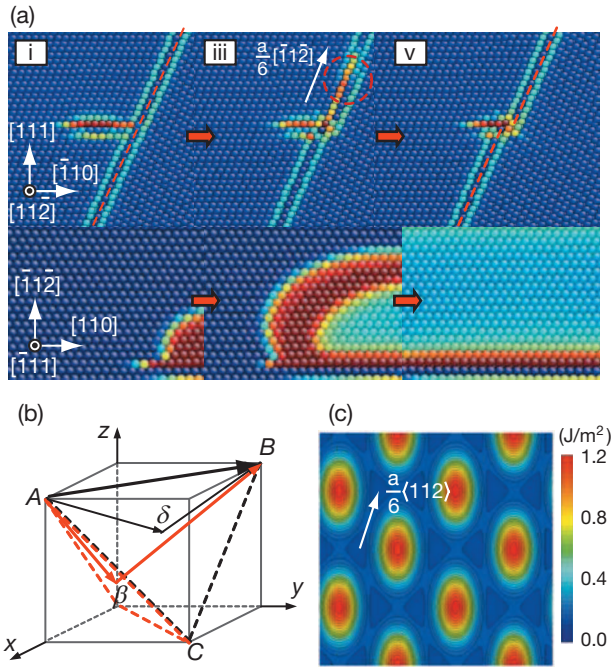

FIG. 3. (Color) Dissociation of a lattice dislocation on the grain boundary. (a) The motion of a misfit dislocation on the grain boundary as viewed in the $[11\bar{2}]$ and $[\bar{1}11]$ directions. (b) Schematic showing the dissociation of a perfect dislocation (AB) into a displacement shift complete (DSC) dislocation ($A\beta$) and a step dislocation (βB) with the Thompson tetrahedron. (c) Energy difference of the grain-boundary slip motion where sixfold symmetry is observed along the MEP.

to $a/\sqrt{3}$. The misfit dislocation glides along the grain-boundary plane like a lattice dislocation. Dislocations in the fcc single crystal split into two partial dislocations, known as the Shockley partial dislocation, before they dissociate into anomalous Burgers vectors on the boundary. For example, the following dissociations result from the stable rearrangement of a dislocation with a Burgers vector $b=a/2[\bar{1}10]$ on the $\Sigma3(\bar{1}11)[110]$ grain boundary:

$$\frac{a}{2}[\bar{1}10] \rightarrow \frac{a}{6}[\bar{1}1\bar{2}] + \frac{a}{3}[\bar{1}11] \quad (AB \rightarrow A\beta + \beta B). \qquad (1)$$

The Burgers vector is certainly preserved during the dissociation processes. The first term on the right-hand side of Eq. (1) has the same vector as the partial dislocation of fcc crystal which lies on the plane parallel to the grain-boundary plane. Figure 3(b) shows the crystallographic orientation of Eq. (1) using the Thompson notation, which indicates that a perfect dislocation AB dissociates into $A\beta$ and βB on the grain boundary. Burgers vector $a/3[\bar{1}11]$ (βB) is the residual component, normal to the boundary plane, which is obviously not on the slip plane in the fcc lattice. Immobilization on the grain-boundary plane results and a far higher-energy barrier is present for successive mobile dislocations. The vector $a/6[\bar{1}1\bar{2}]$ ($A\beta$) is referred to as the DSC dislocation and is defined as a unit lattice translation vector on the CSL

grain boundary. It is known that a lattice dislocation can be absorbed into CSL by dislocation dissociation.[29] Similarly we found that a pure edge dislocation is absorbed into CSL grain boundary through the dissociation into the DSC dislocation and the residual immobile dislocation. When focusing on the DSC dislocation, the energy difference of the slip deformation along the grain-boundary plane is evaluated and shown in Fig. 3(c). A sixfold symmetry exists along the MEP in this figure and thus the DSC dislocation in $\Sigma 3(\bar{1}11)[110]$ slips more easily on the grain-boundary plane [see Fig. 3(a)]. The dissociation of the lattice dislocation results in the disappearance of dislocations beside the grain boundary and the significant grain-boundary migration.[4,5]

In summary, particular attention was given to the activation energy and minimum-energy path, during the interaction process, of the dislocation and the most stable $\Sigma 3(\bar{1}11)[110]$ grain boundary via atomistic transition state analysis. The activation energy for the dislocation–grain-boundary process is calculated to be $\Delta E = 1.16 \times 10^{-1}$ eV/Å. This value is 10^4 times higher than the Peierls potential of a pure edge dislocation and thus the $\Sigma 3(\bar{1}11)[110]$ grain boundary can be a major energy barrier during dislocation motion. We described the dissociation of the lattice dislocation into a DSC as well as an immobile dislocation and determined that the energy difference of the displacement shift on the grain-boundary plane is small. Consequently the dissociation of the lattice dislocation becomes a key factor in the dislocation disappearance beside the grain boundary and also the grain-boundary migration.

The authors T.T. and Y.S. acknowledge recurring financial support from the Japan Society for the Promotion of Science (JSPS), Grant-in-Aid for Young Scientists (Start-up, Grant No. 19860088) (T.T.) and Grants-in-Aid for Scientific Research (S, Grant No. 20226004) (Y.S.). Technical support for parallel computing from the Center for Computational Science and e-Systems at the Japan Atomic Energy Agency is appreciated.

[1] E. O. Hall, Proc. Phys. Soc. London, Sect. B **64**, 747 (1951).
[2] N. J. Petch, J. Iron Steel Inst., London **174**, 25 (1953).
[3] Y. Ikuhara, H. Nishimura, A. Nakamura, K. Matsunaga, T. Yamamoto, and K. P. D. Lagerlof, J. Am. Ceram. Soc. **86**, 595 (2003).
[4] A. M. Minor, E. T. Lilleodden, E. A. Stach, and J. W. Morris, Jr., J. Mater. Res. **19**, 176 (2004).
[5] A. M. Minor, S. A. S. Asif, Z. W. Shan, E. A. Stach, E. Cyrankowski, T. J. Wyrobek, and O. L. Warren, Nature Mater. **5**, 697 (2006).
[6] A. F. Wright and S. R. Atlas, Phys. Rev. B **50**, 15248 (1994).
[7] R. Wu, A. J. Freeman, and G. B. Olson, Science **265**, 376 (1994).
[8] J. S. Braithwaite and P. Rez, Acta Mater. **53**, 2715 (2005).
[9] M. Yamaguchi, M. Shiga, and H. Kaburaki, Science **307**, 393 (2005).
[10] J. D. Rittner and D. N. Seidman, Phys. Rev. B **54**, 6999 (1996).
[11] P. Ballo and V. Slugeň, Phys. Rev. B **65**, 012107 (2001).
[12] T. Richeton, J. Weiss, and F. Louchet, Nature Mater. **4**, 465 (2005).
[13] V. Yamakov, D. Wolf, S. R. Phillpot, A. K. Mukherjee, and H. Gleiter, Nature Mater. **1**, 45 (2002).
[14] J. Schiøtz and K. W. Jacobsen, Science **301**, 1357 (2003).
[15] H. Van Swygenhoven, P. M. Derlet, and A. G. Froseth, Nature Mater. **3**, 399 (2004).
[16] B. J. Pestman, J. T. M. de Hosson, V. V., and F. W. Schapink, Scr. Metall. **23**, 1431 (1989).
[17] M. de Koning, R. J. Kurtz, V. V. Bulatov, C. H. Henager, R. G. Hoagland, W. Cai, and M. Nomura, J. Nucl. Mater. **323**, 281 (2003).
[18] K. J. Kim, J. H. Yoon, M. H. Cho, and H. Jang, Mater. Lett. **60**, 3367 (2006).
[19] Z. Jin, P. Gumbsch, K. Albe, E. Ma, K. Lu, H. Gleiter, and H. Hahn, Acta Mater. **56**, 1126 (2008).
[20] G. Henkelman, B. P. Uberuaga, and H. Jónsson, J. Chem. Phys. **113**, 9901 (2000).
[21] Y. Mishin, D. Farkas, M. J. Mehl, and D. A. Papaconstantopoulos, Phys. Rev. B **59**, 3393 (1999).
[22] T. Tsuru and Y. Shibutani, Phys. Rev. B **75**, 035415 (2007).
[23] G. Kresse and J. Hafner, Phys. Rev. B **47**, 558 (1993).
[24] G. Kresse and J. Furthmuller, Phys. Rev. B **54**, 11169 (1996).
[25] J. P. Perdew, J. A. Chevary, S. H. Vosko, K. A. Jackson, M. R. Pederson, D. J. Singh, and C. Fiolhais, Phys. Rev. B **46**, 6671 (1992).
[26] H. J. Monkhorst and J. D. Pack, Phys. Rev. B **13**, 5188 (1976).
[27] J. Li, Modell. Simul. Mater. Sci. Eng. **11**, 173 (2003).
[28] W. A. T. Clark and D. A. Smith, J. Mater. Sci. **14**, 776 (1979).
[29] D. J. Dingley and R. C. Pond, Acta Metall. **27**, 667 (1979).